Alkali-activated mortars: porosity and capillary absorption

Moussa Ka, David Hoffmann, Laurent Molez, Christophe Lanos

Alkali-activated mortars: porosity and capillary absorption

Moussa Ka[a], David Hoffmann[b], Laurent Molez[c] and Christophe Lanos[a]

[a]Universitè de Rennes, LGCGM, France; [b]Hoffmann Green Cement Technologies, Chaillè sous les Ormeaux, France; [c]Universitè de Rennes, INSA Rennes, LGCGM, Rennes, France

ABSTRACT

Studies conducted on alkali-activated materials in late years attested that they could be a replacement to ordinary Portland cement (OPC). Nevertheless, their performances in aggressive conditions require profound investigations to evaluate the ability to the fluid transfer. This article assesses the pore structure of alkali-activated mortars produced using one- part metakaolin combined with ground granulated blast furnace slag and other-part using only alkali-activated ground granulated blast furnace slag. The pore characteristics of alkali-activated mortars were compared to those of OPC as a reference. Tests consist in the measurement of the porosity accessible to water, water absorption and sorptivity. The results revealed that the alkali-activated based metakaolin combined with ground granu- lated blast furnace slag have greater porosity, water absorption, sorptivity and rate of water saturated porosity than alkali-activated based ground granulated blast furnace slag and Portland cement mortars.

KEYWORDS

Alkali-activated mortar; ground granulated blast furnace slag; metakaolin; porosity; sorptivity

1. Introduction

Today the construction sector is encountered with the gradual depletion of natural resources and growing difficulty in accessing them, but also the large quantities of CO_2 emitted for the manufacture of cement. In 2018, the global cement output reached 82,000 million tons, including 35,700 million tons in China, 12,460 million tons in the United States and 25,640 million tons in Europe (Bildirici, 2019; Hagemann et al., 2019). About 8% of total CO_2 emissions are assigned to ordinary Portland cement (OPC) production (Andrew, 2018; Zhang et al., 2014). In the context of climate change horizon, alkali-activated materials (AAM) seem to provide an effective alternative to OPC cement (Pacheco-Torgal et al., 2012) and because most of them are manufactured with industrial by-products. That is why in late years their development has created the interest of the scientific community.

AAM are fabricated from a mixture of aluminosilicate raw materials activated by an alkaline solution (Mackenzie & Welter, 2014). These materials can be separated into two main categories according on the calcium content of the raw materials (Li et al., 2010). When the calcium content is low, the AAM produced are named geopolymers. Geopolymers are obtained by reaction between solid precursors such as metakaolin, fly ash with an alkaline activator. The product obtained from this reaction is formed for a gel type N-A-S-H (Na_2O-Al_2O_3-SiO_2-H_2O) (Gao et al., 2015). They have polymeric structure that is why Davidovits calls them “geopolymer” (Davidovits, 1994). Geopolymerisation is a procedure where the vitreous components of the aluminosilicate source materials are transformed into a compact binder (Fernandez et al., 2006). When the calcium content is very important in the used raw material, the reaction product is formed by a gel type C-A-S-H (CaO-Al_2O_3-SiO_2-H_2O). Ground granulated blast furnace slag (GGBFS) is a raw material with a high content of Ca. It is well known that GGBFS has high pozzolanic activity and can be alkali activated (Shi & Qian, 2000). The quantity of CaO content of the precursor materials was found to have significant impact on the resulting hardened geopolymer. Decrease in set- ting time and increase in strength was quoted with the increase of CaO content (Diaz et al., 2010). Many investigations have recently been made on the effect of calcium on geopolymerisation (Granizo et al., 2004; Yip et al., 2005, 2008). In both cases, the reaction mechanism is very different. Despite of the differences in nanostructure and constitution between N-A-S-H and C-A-S-H, both gels are estimated to have very good physicochemical and mechanical durability properties (Duxson et al., 2005; Provis & van Deventer, 2014). The reactivity of AAM is influenced by several parameters. These parameters include: fineness, mineral composition and morphology. Shi et al. (2006) have detailed the general properties of slag and metakaolin in their work on alkali-activated cements and concretes. In their book, Provis and Van Deventer (2009) summarised the different properties of the raw materials used in the manufacture of geopolymers.

Durability is a high concern for building materials. To study the compressive strength and sorptivity characteristics of a high performance GGBFS-based concrete, Sarathy and Dhinakaran (2014) conducted experimental research. These researchers found that concrete with GGBFS and manufactured sand gave better results than the traditional mix, both in terms of sorptivity and compressive strength. Hall and Yau (1987) studied the sorptivity in concrete and they showed how the sorptivity varies in a set of concrete samples of different mix and different degrees of compaction. The materials respond to moisture around them by absorbing water as vapor or liquid, redistributing it, and under drying conditions breathing it back into the air. The authors showed that a low water/binder ratio decreases the sorptivity of the materials and that careful compaction leads to higher sealing and lower sorptivity. Their results confirm those of Gu et al. (2022) who showed that a more homogeneous and compact microstructure improves the durability of magnesium oxysulfate cement under air hardening conditions.

Hall (1989) showed that all simple water absorption test procedures in principle furnish data from which the sorptivity can be estimated. Borges et al. (2016) have studied the apparent porosity for the blended metakaolin/blastfurnace slag alkali-activated mortars calculated from the water saturation method and from mercury intrusion porosity (MIP). Overall, the water saturation method gave higher porosity results. According to Aligizaki (2005), the porosities measured by the water saturation method are higher than the porosities by MIP for cement pastes because the gel pores absorb water and swell during the saturation process, altering the results. This phenomenon appears to happen in alkali-activated systems as well. Borges et al. (2016) have shown similar pore size distribution for all mortars, irrespective of the precursors used [metakaolin (MK) or MK/BFS] or composition of the matrices (SiO_2/Al_2O_3 or R SiO_2/Na_2O). Most curves present a bimodal pore distribution, with significant porosity between 10 and 100 nm and between 1 and 10 mm. This broad pore size distribution is typical for mortars and concretes, both of which with MIP results that differ from pastes (Cook & Hover, 1993).

More understanding regarding pore size and pore distribution are needed for AAM mortars based metakaolin combined with ground granulated blast furnace slag. This article presents a study of durability parameters of AAM materials such as porosity, capillarity and sorptivity. In this study, ambient cured mortars, i.e. AAM employing ground granulated blast furnace slag (GGBS) as solid raw materials, meta- kaolin–granulated blast furnace slag (MK-GGBS) alkali activated and Portland cement (PC) mortars were produced. The results of this work might be precious for the development of sustainable materials.

2. Materials and experimental methods

2.1. Components

Four different binders including ground granulated blast furnace slag (GGBFS), metakaolin, ettringitic addition and cement were used as components of the mixes. Granulated blast furnace slag was supplied by Ecocem (Fos-sur-Mer (France)). Metakaolin type Argicem is provided by Argeco (France) and sulfo-aluminate binder Alicem supplied by Ciments Calcia (Italie). In this study, the Portland cement used is a CEM I 52.5 N (Lafarge – Le Teil (France)). The sand used in all formulations of the mortars is an alluvial quartz sand with a grain size 0/2. Superplasticizer Tempo 12 from Sika (Switzerland) was used to ensure sufficient flow of mortar and limit the segregation. In all formulations, tap water is used for the preparation of mortars.

The elementary composition of the GGBFS, metakaolin, ettringitic addition and Portland cement are determined by X-ray fluorescence (XRF). Density and fineness of binders is determined on powder using a Blaine permeameter. The power X-ray diffraction pattern is recorded using a Panalytical X'PERT PRO MD diffractometer equipped with a Ni-filtered Cu (45 kV–40 mA) Panalytical anti-cathodic tube (k 1.54 Å) and a high-resolution TRMS Panalytical X'Celerator fast detector in scanning mode (2.2 mm active length). Recording is performed between 5^0 and 75^0 in $2h$. A laser particle size analyser was used to determine the particle size distribution of components.

The elementary composition of the slag, metakaolin, ettringitic addition and cement determined by XRF are given in Table 1. This table shows that the slag and the cement contain the most quantities of silica and calcium responsible of the pozzolanic reaction, but the quantity of calcium of metakaolin is very small.

Table 1. Chemical composition of the metakaolin, ettringitic addition, slag and cement (wt%).

	Precursors			
Chemical composition	Metakolin	Ettringitic addition	GGBFS	Cement
SiO_2	55	6.7	37.3	20.4
Al_2O_3	40	24.1	10.2	5.5
CaO	0.3	37.3	43.2	64.2
MgO	0.2	–	6.1	1.70
Fe_2O_3	1.4	1.2	0.6	2.1
TiO_2	1.5	0.7	0.5	0.2
K_2O	0.8	0.6	0.6	0.4
SO_3	–	26.6	0.1	3.2

The physical properties of ground granulated blast furnace slag, metakaolin, ettringitic addition and cement are presented in Table 2. The table shows that the metakaolin with a 2.5 of density is much lighter than other precursor materials. It has also a high-specific Brunauer, Emmett et Teller (BET) surface of 15.65 m^2/g. The specific surface of the metakaolin is very high and much higher than that of other binders. Indeed, this metakaolin is conventionally used to promote pozzolanic reaction in Portland cement concrete.

Figure 1 shows the particle size distribution of the four precursor materials. These results showed that ettringite addition is much finer than the metakaolin, slag and cement. According to these results it is found that the granulometric curve of the metakaolin corresponds to coarse grains while the specific sur- face is very important. The morphology of the metakaolin is usually close to the morphology of the starting kaolinite, the latter being in the form of hexagonal sheets contiguous to each other and a thickness of a few Angstroms, which explains this lack of dispersion.

Figure 2 presents the XRD patterns of metakaolin, ettringitic addition, cement and ground granulated blast furnace slag. In the ettringitic addition, calcium sulfate ($CaSO_4$) and calcium aluminum oxide sulfate ($Ca_4Al_6O_{12}SO_4$) are the main crystalline phase. Calcium silicate (Ca_3SiO_5) and gypsum ($CaSO_4.2H_2O$) are the main crystalline in the cement. The metakaolin contained large amounts of impurities such as quartz (SiO_2), kaolinite ($Al_2Si_2O_5(OH)_4$ and muscovite ($KAl_2(AlSi_3O_{10}(OH,F)_2$). The XRD patterns of GGBS indicate that the majority of ground granulated blast furnace slag is practically completely amorphous. It is assumed to be 100% glassy.

The mixes include soda obtained by dissolving dry caustic pellets in water (to obtain 32% NaOH concentrated solution) or commercial VWR (Company specializing in the sale of products and services for Life Sciences and regulated industries) sodium silicate N (containing 26.3 wt% SiO_2, 7.9 wt% Na_2O and 65.8 wt% H_2O). In the case of sodium silicate, alkaline-activating solution was pre-formulated by mixing the sodium silicate with the NaOH solution. This leads to a partial dissolution of the silica. The alkaline solution is cooled at room temperature for 24 h before the manufacture of mortars.

2.2. Sample preparation

Table 3 shows the mix proportions of the cement mortar and mortars based on metakaolin combined with ground granulated blast furnace slag and the corresponding molar rations SiO_2/Na_2O for AAM binders. Table 4 shows the mortars mix proportions based only on ground granulated blast furnace slag. The ratio *W*/*B* (total water content to binder) and the ratio *S*/*B* (sand to binder) are indicated. These molar ratios are calculated assuming a total dissolution of the silicon and sodium from the activator. Samples with alkali-activated binders based on metakaolin combined with ground granulated blast furnace slag are denoted G001 and G002 respectively. The ettringite addition is used to regulate the setting. Samples with alkali-activated binders based only on ground granulated blast furnace slag (without metakaolin) are denoted U001 and U002 respectively. C001 corresponds to the reference Portland cement mortar.

Table 2. Physicals properties of the precursors materials.

Physical properties	Metakaolin	Ettringitic addition	Slag	Cement	Sand
Specific surface area (m^2/g)	15.65 BET	0.5 Blaine	0.42 Blaine	0.35 Blaine	–
Density (g/cm^3)	2.52	2.75	2.76	2.94	2.64

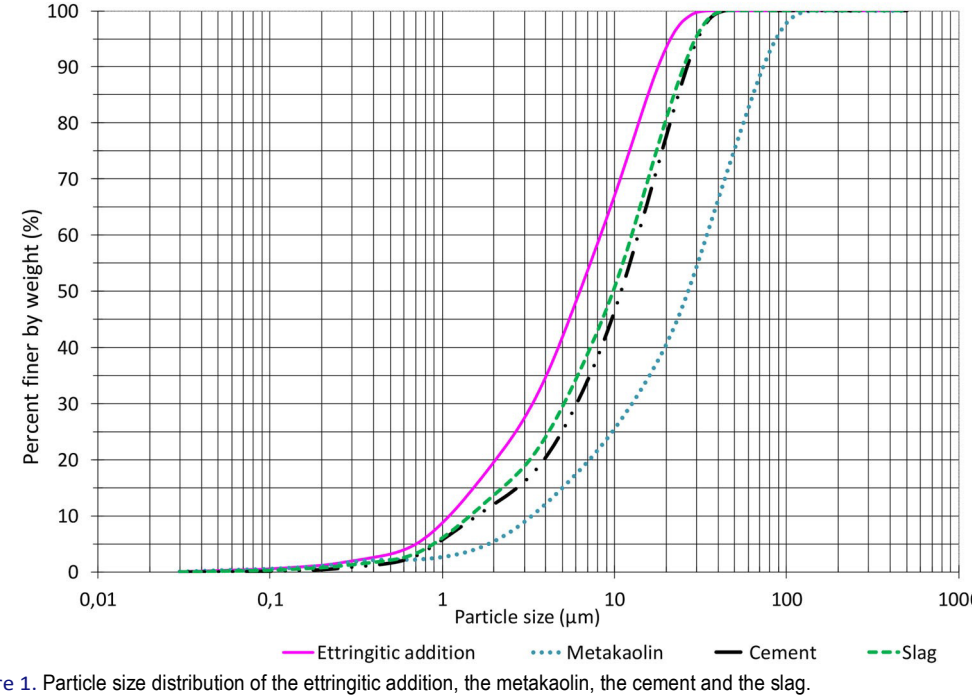

Figure 1. Particle size distribution of the ettringitic addition, the metakaolin, the cement and the slag.

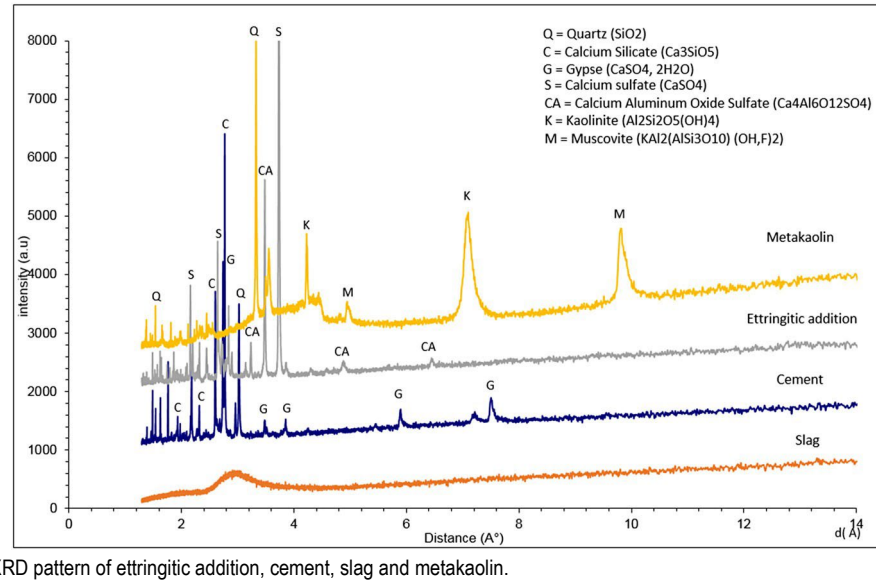

Figure 2. XRD pattern of ettringitic addition, cement, slag and metakaolin.

Table 3. Mix proportions of the cement mortar and mortars based on metakaolin combined with ground granulated blast furnace slag (in g for the same sand content).

	C001	G001	G002
Metakaolin	–	300	450
GGBFS	–	45	43
Ettringitic binder	–	–	21
Portland cement	450	–	–
Sand 0/2	1350	1350	1350
Sodium silicate N	–	210	298
Soda 32%	–	135	160
Tempo 12		4.0	5.6
Added water	225.0	–	–
SiO_2/Na_2O		1.14	1.28
W/B	0.50	0.51	0.46
S/B	3.00	3.00	2.06

Table 4. Mix proportions of the mortars based on ground granulated blast furnace slag (in g for the same sand content).

	U001	U002
GGBFS	412	412
Sodium metasilicate	66	66
Sand 0/2	1350	1350
Sodium fluoride		5
Sodium carbonate	5	
Added water	190	190
W/B	0.40	0.40
S/B	2.82	2.82

For activated slags, additives have been added. Their role is to prevent the penetration of water and impregnate the pores. It appears that the use of sodium carbonate increases drastically the setting time whereas the sodium fluoride accelerates the setting.

The mortars were prepared in two steps. First, pure NaOH and water were added to the industrial waterglass solution to obtain the desired SiO_2/Na_2O molar ratio. After the total dissolution of the sodium hydroxide, the solution was cooled to 20 ^{0}C for 24 h.

The mortars were mixed and made according to French standard EN 196-1 (NF EN 196-1, 2005) using the activation solution instead of the mixing water. The precursors are mixed with the activation solution. In all formulations, the volume of paste is not constant. Standard sand having a controlled particle size between 0 and 2 mm was used. The mortar specimens were cast in 40x40x160 mm PolyVinyl Chloride (PVC) moulds using a shock table. All specimens were cured at 20 ^{0} C and 95% R.H. for 24 h and then demoulded and stored under the same conditions until testing.

2.3. Tests methods

2.3.1. Open porosity

Open porosity measurements consist in the evaluation of the voids volume connected to the mortar sur- face. Tests are realised on prismatic specimens aged 28 days. The mortar samples are sawed to obtain two half-prismatic samples. Later, the half samples are dried at 60 ^{0} C until a constant weight was achieved (W_d). The mass is considered constant when the difference between two measurements in 24 h is <0.2%. The half samples are then placed in a sealed desiccator. Using a vacuum pump connected to the device, the pressure is reduced to reach 100 mbar. Vacuum is maintained for 4 h, then water was gradually introduced until sample immersion. The reduced pressure is maintained for 44 h and then the container was opened. At the end of this step, a weighing in the air (W_a) is carried out followed by a hydrostatic weighing (W_w) of the samples. Finally, the open porosity accessible to water is calculated:

$$p = 100\,(W_a - W_d)/\,(W_a - W_w)$$

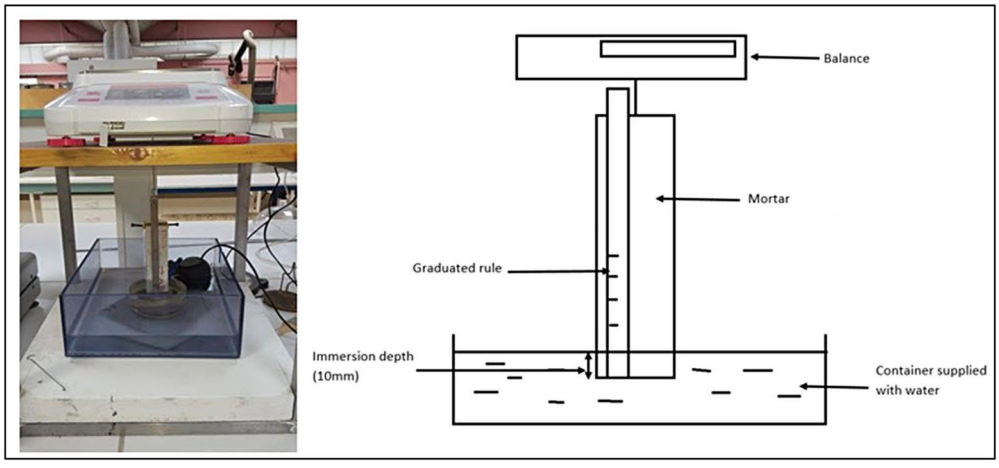

Figure 3. Capillary absorption test.

2.3.2. Capillarity absorption, sorptivity and pore structure analysis

Capillary absorption of the mortars prims specimens (40 mm x 40 mm x 150 mm) is carried out on a test device made in the laboratory (see Figure 3). Samples are first rectified. They are sawed 0.8 cm on one of their ends to obtain a characteristic absorption surface representative of the heart of the sample. Mortar specimen is dried at 60 ^{0}C until this weight became constant (the mass is considered constant when two successive weightings carried out at 24 h apart do not differ by more than 0.05% between them). All the lateral and upper surface of the sample is sealed using adhesive aluminum paper to avoid any phenomenon of water evaporation. One of the lateral surface is coated with a transparent waterproof film to visually record the height of the water rising. A graduated ruler is placed on this face to evaluate the absorption height. The dried sample mass is measured after preparation (W_d). The sample is then suspended under an electronic scale. Sample base is placed in a container filled with water using a water pump to maintain by mean of overflow a submerged height of 10 mm. The sample mass evolution is recorded from the start of immersion until 24 h. The sample mass (W_w) is conventionally measured after 15, 30 min and then 1, 2, 4, 8 and 24 h of immersion. At each term, the height (H_w) of the capillary front is quoted using the graduated ruler.

A water pump powered the system to drop the water level until constant immersion is high. When the contact of the sample with water occurs, during the first few seconds, the apparent mass of the sample decreases. Archimedes' principle explained this fact. At the beginning of the test, effect of buoyancy increases due to the elevation of water level in the cup and at the same time decreases as the water fill the accessible open porosity of immersed part of the sample and absorbed by capillarity in the emerged part of the sample. As a consequence, the apparent mass of the sample decreases initially, then goes through a minimum value and finally increases. This phenomenon must be taken into account to interpret the results. The initial value of the capillary coefficient has no meaning.

Estimating a negative capillary coefficient at the beginning of the test is not interesting. An example of sample mass tracking as a function of time (logarithmic basis) is given in Figure 4. The data registered until 24 h of test are used to characterise the capillary absorption.

For the characterisation of the mortars, capillary absorption, sorptivity and pore structure analysis are evaluated.

The capillary absorption of the mortars specimens is calculated using:

$$C_a = (W_w - W_d)/\,S$$

where S is the absorption surface in square meter (m^2).

The capillary absorption is conventionally evaluated after 24 h of immersion.

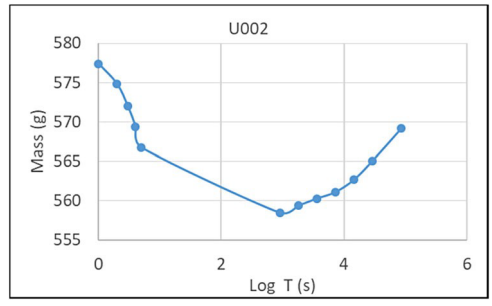

Figure 4. Mass evolution of the U002 alkali-activated slag mortar during the capillary absorption.

In this study, beyond 15 min, the absorption capillary at different time intervals follow a linear progression as a function of the square root of time which makes it possible to characterise each specimen by a value of sorptivity.

According to standard NF EN 13057 (2005), the sorptivity expressed in (kg m-2 h-1/2) is calculated between 1 and 8 h of test. In their sorptivity calculation, Hall and Tse (1986) used this same time interval. Mermerdas¸ et al. (2017) consider that sorptivity can be considered as one of the easier test for evaluating permeability of mortar. These researchers showed that water could penetrate into the mortar specimens by capillary suction. In fact, Balayssac (1993) showed that two parameters can be released from these plots. In Figure 5, the first part of the curves located between 0 and 1 h reflects the filing of the largest pores. These larger pores can be characterised from the initial absorption in zone A of Figure 5 (amount of water absorbed between 0 and 1 h). This initial sorption is due also to rapid saturation of capillary pores. The second part of the curve (zone B), which extends beyond one hour, characterises the filing the internal capillaries, this filing process is made of the largest capillaries in the finest.

Hall (1989) showed that sorptivity measurement can be made with any wetting fluid and that the sorptivity as classically measured is the water sorptivity or hydraulic sorptivity. This technique uses pure water as an absorbed fluid.

The height (H_w) of the capillary front and the water mass absorbed by capillarity can be used to evaluate the porosity distribution versus the equivalent radius of the capillary. According to the law of Jurin, which stipulates that by capillarity a liquid rises in a tube up to a height h given by the formula below, we can connect the capillary rise to the pores diameter as follows:

$$h = (2\,\gamma \cos\theta)/\,(r\,\rho\,g)$$

with:

h the height of the liquid above the water level in m,

γ the surface tension of the liquid in N m-1. By hypothesis, the surface tension was estimated at 73 x 10^{-3} N m^{-1}, corresponding to the surface tension of pure water at 20 °C. In cements and geopolymers, this tension can be different due to the solubility of the basics ions.

θ the wetting angle between the liquid and the tube wall. The value chosen is 0°C. The contact angle of a fluid on a surface depends on the nature of the surface. It is not certain that this value is the same for a geopolymer, an alkali-activated slag or a cement.

ρ is the density of the liquid in kg m^{-3},

r is the diameter of the tube in m,

g is the acceleration of gravity, it is a constant worth about 9.81 m s^{-2} .

The assumption linked to this calculation is strong. The pore size calculation is based on perfect tubular pores and using static-state calculation. Therefore, the results are not intrinsic and can be only used for comparison.

However, under these conditions, the wetting angle is not known, which leads us to estimate an absorption range by calculating the radius r of the sample by its final radius r_f.

On the other hand, using the measurements of capillary absorption, it is possible to evaluate from Δm the absorbed water volume trapped into the filled pore at all times. Using the inhibition front position h the water saturated porosity of the mortars can be calculated at all times. Using the law of Jurin and Δh, the variation of height corresponding to the filing of finer pores, the range of pore radius filled by water can be evaluated at all times. Details are presented in Figure 6.

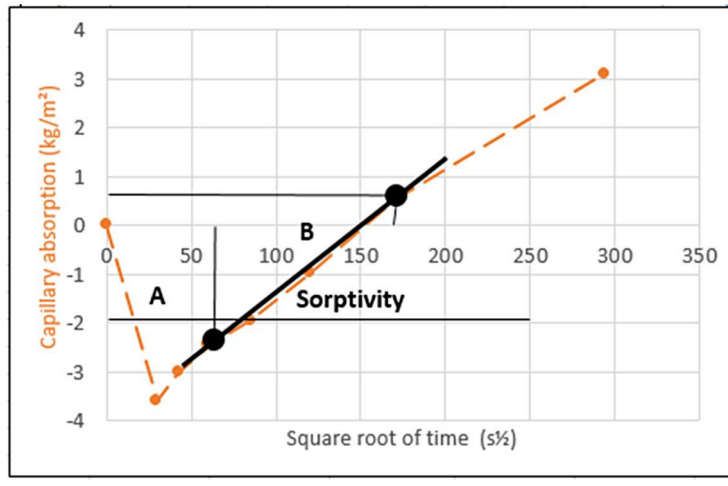

Figure 5. Example of the schematic representation of the sorptivity (expressed in kg m^{-2} $h^{-1/2}$) of U002 mortar.

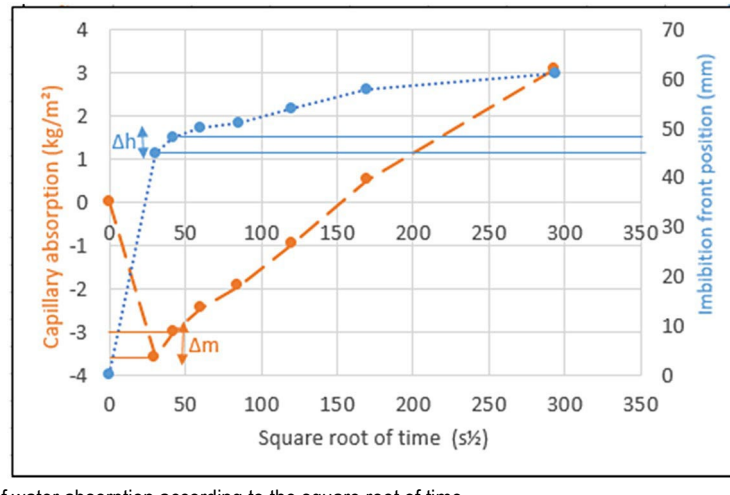

Figure 6. Kinetics of water absorption according to the square root of time.

3. Results and discussions

3.1. Open porosity

The porosity results obtained at 28 days (average of two measurements) are shown in Figure 7 and Table 5.

The porosity of the Portland cement mortar C001 was about 14%. The porosities of the AAM realised with sodium silicate G001 and G002 are respectively 19.3% and 21.5%. Their porosity is higher than C001. G001 presents a same *S*/*B* ratio than C001 but higher porosity showing that this AAM paste is more porous than Portland cement paste. Introducing ettringitic binder (G002) but with lower *S*/*B* ratio than G001 leads to increases in porosity. Effect of ettringitic binder on porosity is not clear.

This increase in the water absorption and porosity of the AAMs could be due to the voids or fissures that occurred during the initial condition of the samples for this test (i.e. oven curing at 60 ^{0}C till a constant mass was achieved). The formation of these voids/fissures would result in a corresponding increase in the water absorption of the AAMs.

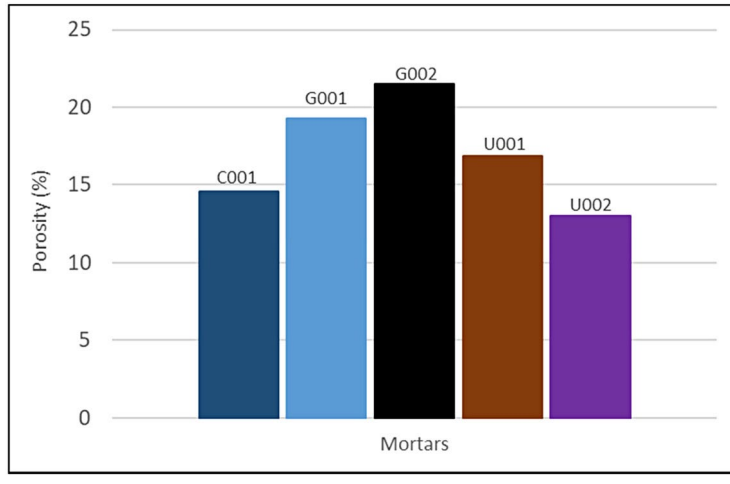

Figure 7. Porosity of mortars at 28 days.

Table 5. Porosity, capillary absorption, imbibition front position and sorptivity data of the alkali activated materials.

	W/B	Porosity (%)	Capillary absorption after 24 h (kg m^{-2})	Imbibition front position after 24 h (mm)	Sorptivity between 1 h and 8 h (kg m^{-2} $s^{-1/2}$)	Water saturated porosity after 24 h (%)
C001	0.50	14.6	07.1	50	0.030	14
G001	0.51	19.3	13.0	61	0.050	21
G002	0.46	21.5	13.4	56	0.054	24
U001	0.40	16.9	11.2	81	0.041	14
U002	0.40	13.0	06.7	61	0.029	11

U001 and U002 mortars based on activated slag present a porosity (16.9% and 13.0%) close to the Portland cement mortar C001 (with close *S*/*B* but lower *W*/*B*). Substitution of sodium carbonate by sodium fluoride allows to reduce the porosity. Unfortunately, the use of sodium fluoride increases drastic- ally the setting time whereas the sodium carbonate accelerates the setting. The results showed that the onset of setting time of mortar U001 is 40 min and its end of setting time is 95 min. However, the start of setting time for mortar U002 is 130 min and its end of setting time is 265 min. It is thus observed that the setting time does not depend solely on the quantity of water present in the two mixtures. Mortars U001 and U002 have the same water/binder ratios ¼ 0.40 but very different onset times. This difference can be attributed to the additives used.

Such results are in accordance with those of Al-Otaib (2008). He reported in his study that alkali-activated slag concrete has higher porosity value compared with cement Portland. He obtained a range of porosity of 13%–10% at the age of 7–360 days, while Portland cement concrete showed a porosity of 10.4%–8% for the same age.

These results show that GGBS mortars with additives greatly reduce the porosity accessible to water. Provis et al. (2012) show that slag in AAM decrease the total porosities when slag content reach 70%. They showed that this difference is due to the better space filling effect of C-A-S-H gel than N-A-S-H.

3.2. Capillarity absorption, sorptivity and pore structure analysis

3.2.1. Capillarity absorption

The capillary absorption curves presented in Figure 8 and in Table 5 are arbitrarily drawn starting from data measured at 15 min. This figure shows that between 15 min and 24 h, all the tested mortars present the same behavior. The curves are quite linear and the capillary absorption at 24 h can be used for the discussion.

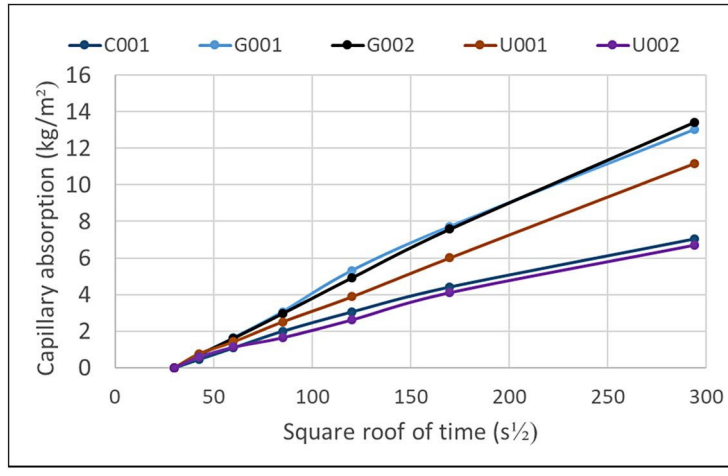

Figure 8. Capillary absorption evolution of the specimens.

The Portland cement mortar presents a capillary absorption at 24 h of 7.1 kg m^{-2}. G001 and G002 AAM have higher absorption (respectively 13.0 kg m^{-2} and 13.4 kg m^{-2}) than all others mortars. This result can most likely be attributed to their high porosity (respectively 19.3% and 21.5%) favoring their water absorption. In fact, water absorption is related to the open porosity. The introduction of ettringitic addition in G002 does not lead to drastic change in the capillary absorption. Higher water absorption of AAMs mortars at 28 days could be also due to the slow process of geopolymerisation.

At 24 h, the capillary absorption of U001, U002 based on activated slag are respectively 11.2 kg m^{-2} and 6.7 kg m^{-2}. The low U002 mortar capillary absorption is partly due to a lower porosity and to effect of the additive. A repellent effect of sodium fluoride can be suspected. This low in the water absorption can be attributed to increase in pozzolanic reaction, higher degree of geopolymerisation and filler effect due to addition of additives as time progresses, which can help to densify the micro- structure of mortars by increasing the amount of hydration products and by filling the micropores and microcracks. Water absorption of the present study showed good agreement with the study conducted by Mermerdas¸ et al. (2017), where water absorption of two-part FA-based AAM varied from 8% to 11%.

Adam (2009) found that the capillary absorption of the alkali-activated slag concrete did not perform well. Chi and Huang (2013) studied the effect of cement, fly ash and slag on water absorption. These researchers obtained water absorption of 7.5% for cement Portland mortar, but they found that absorption reduced considerably for the alkali-activated binder (1.1%–6.1%). These researchers showed that this decrease depends on the ratio of slag-to-fly ash and activator contents.

3.2.2. Sorptivity

Figure 9 shows the water sorptivity of different specimens estimated between 1 h and 8 h (values in Table 5). These results showed that specimens G001 and G002 have very high sorptivity equal to 0.05 kg m^{-2} $s^{-½}$ and 0.054 kg m^{-2} $s^{-½}$ respectively. Their sorptivity are higher than that of C001 that was 0.030 kg $m^{-2}/s^{-½}$. The addition of ettringitic does not modify the sorptivity.

The sorptivities of U001, U002 and C001 are 0.041 kg m^{-2} $s^{-½}$, 0.029 kg m^{-2} $s^{-½}$ and 0.030 kg m^{-2} $s^{-½}$ respectively. We observe that U002 and C001 have approximately the same sorptivities. Their difference in *W*/*B* and additives type did not have a significant effect on their sorptivity. These results indicate that the capillary forces of U002 AAM transport less water than U001 mortar. This phenomenon demonstrated that U002 mortar is more sustainable and durable in regard to limiting the water access (Albitar et al., 2017). This phenomenon is partially attributed to the difference in the capillary mechanism and the size pore distribution.

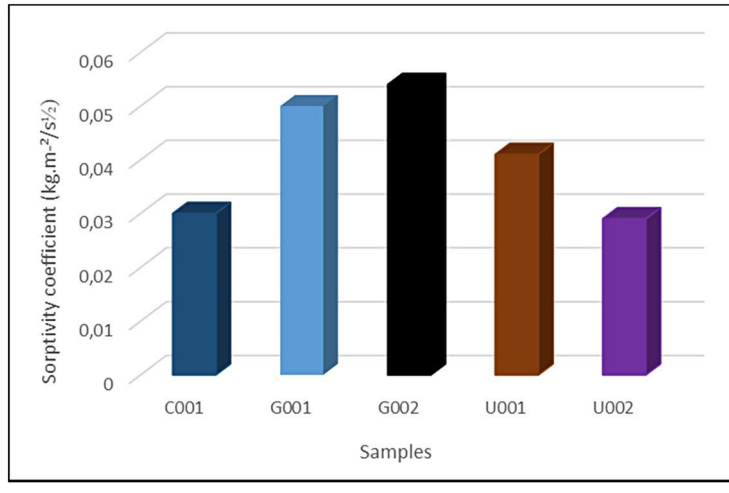

Figure 9. Sorptivity of different specimens between 1 h and 8 h.

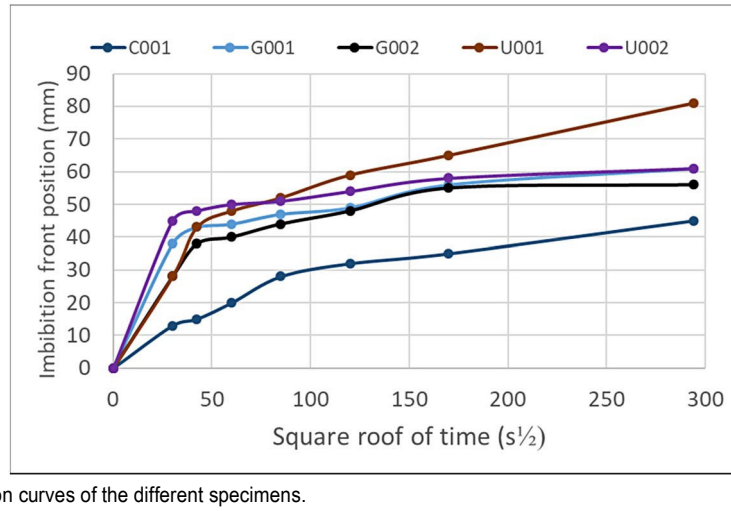

Figure 10. Imbibition curves of the different specimens.

The addition of sodium fluoride significantly improves the impermeability of mortars by reducing porosity, connectivity and inducing hydrophobic surfaces. The increase in the amount of additive causes a decrease in the sorptivity. These results showed that additive has strongly modified the microstructure of mortars. This phenomenon is reflected in an improvement of the sorptivity.

3.2.3. Structure pore analysis

The imbibition curves for the different specimens are presented in Figure 10. The capillary absorption and imbibition curves for the different specimens presented in Figures 8 and 10 show that all curves tend towards a stabilisation of the capillary rise while the weight can continue to grow. The progressive filing of the macro porosity (occluded air) can justify this phenomenon. Generally, the secondary absorption (Figure 5B) is controlled by the air voids whereas the capillary forces control the initial absorption (Figure 5A). Capillary absorption and imbibition front results allow to calculate the water saturated porosity and the corresponding r/r_f ratio.

Figure 11 shows the water saturated porosity of the materials according to the r/r_f ratio where r is the finer filled radius for a given time and r_f the finer filled radius obtained at the end of the test (after 24 h). The start of the test corresponds to large values of r/r_f as the end of the test corresponds to $r/r_f = 1$.

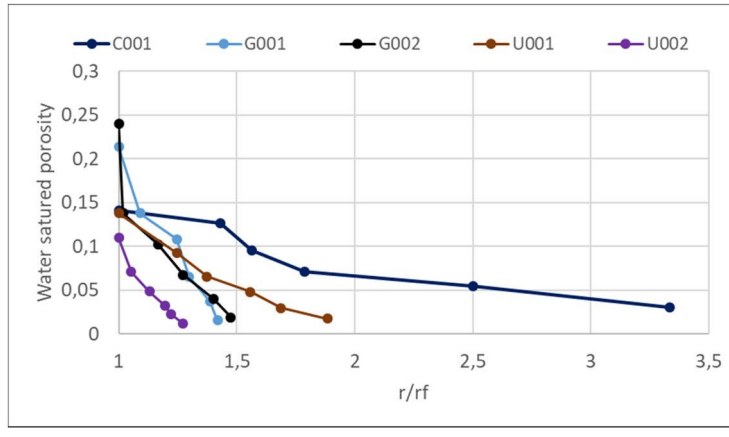

Figure 11. Water saturated porosity of specimens.

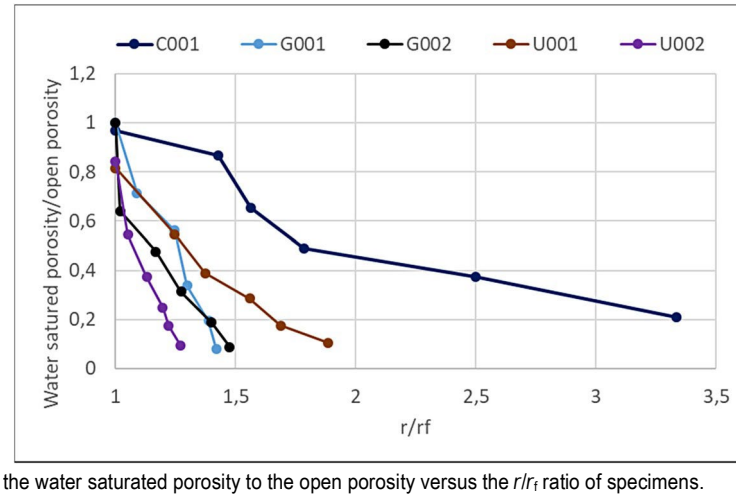

Figure 12. Rate of the water saturated porosity to the open porosity versus the r/r_f ratio of specimens.

The obtained curves are highly indicative and using r/r_f, the strong hypothesis required to perform the filled radius calculation (surface tension and wetting angle must be measured as they probably differ for each mortar) are not necessary. However, the calculation does not take into account any dynamic effect such as phenomenon of slow filling of the pores.

For C001 (Portland cement mortar), the water saturated porosities evolves quite linearly with the r/r_f ratio while a large curvature of the curves obtained for alkali-activated binder is quoted.

The maximum water saturated porosity is 14% for C001, 21% and 24% for G001 and G002 alkali-activated mortars respectively. We notice that G002 has the higher water saturated porosity. However, we note that G001 is characterised by quite range of r/r_f ratio.

For U001 and U002, alkali-activated slag mortars, the water saturated porosity is 14% and 11% respectively. According to Provis et al. (2012), the presence of fine particles of slag reduced the filled radius range. U001 and C001 mortars present the same water saturated porosity, but different range of r/r_f ratio. The low U002 mortar water saturated porosity is partly due to a lower porosity and to the effect of the additive. A repellent effect of sodium fluoride can be suspected. Alkali activators except sodium fluoride are strong acid salt whose pH is more than 12. Sodium fluoride is ionised into Na^b and F^-. And F ion absorbs H ion, then becomes acid. Although hydrogen exponent (pH) change of sodium fluoride based binder was decreased with HF concentration, binder was hardened (Song et al., 2010). Although hydrogen exponent (pH) of sodium fluoride activated mortar is about 10, sodium fluoride could accelerate hydration ground granulated blast furnace slag (GGBS) (Song et al., 2010).

Hence, it can be concluded that the inclusion of this additive imparted positive results on U002 mortar by densifying the microstructure due to this chemical (formation of addition hydration products and increase in geopolymerisation process) and physical effects (filling the microcracks and micropores in the AAM mortar).

The water saturated porosity can be compared to the open porosity measured for each type of mortar. The results are presented Figure 12 showing the evolution of the ratio of the water saturated porosity to the open porosity versus the r/r_f ratio. At 24 h, the ratio of water saturated porosity for C001 (Portland cement), G001 and G002 alkali-activated mortars is very close to 1. This means that the open porosity of these mortars are completely filled with imbibed water. Capillary forces are sufficient to saturate all the open porosity. The ettringite addition in G002, the finer particle among the binders (Figure 1), did not prevent the complete pore filling.

The r/r_f ratio obtained for U001 and U002 alkali-activated slags mortars are 81% and 84% respectively. The filling of the open porosity is not complete but remains important. Capillary forces are not sufficient to saturat1e all the open porosity.

4. Conclusion

This article presents the results of an experimental study based on the measurement of the porosity, the capillary absorption, the sorptivity and the water saturated porosity of different alkali activated mortars. The interpretation of these data made it possible to characterise the pore structure of the different mortars and thus underlines the differences in morphology. Based on the results obtained and their discussions, the following conclusions are highlighted.

For mixes of metakaolin and ground granulated blast furnace slag:

- The porosity of such alkali-activated mortars is higher than Portland cement mortar with the same W/B ratio. This higher porosity favors the water absorption and increases the sorptivity.
- Introducing ettringitic binder leads to increases in the porosity even with lower *S*/*B* ratio but does not lead to drastic change in the capillary absorption and sorptivity. The pore structure of this AAM mortar is characterised by a shorter range of r/r_f ratio than Portland cement mortar. At 24 h, the ratio of water saturated porosity is very close to 1 showing that the porosity is well connected.

For mixes of activated ground granulated blast furnace slag:

- The porosity of such mortars is close to those of Portland cement mortar.
- The pore structure of such AAM mortars is characterised by a shorter range of r/r_f ratio than Portland cement mortar. However, the water saturated porosity is close to those of Portland cement mortar.
- The substitution of sodium carbonate by sodium fluoride reduces the porosity, the capillary absorption and the range of r/rf ratio. However, the sorptivity is only slightly reduced.

This study highlights that ground-granulated blast furnace slag activated materials may provide improved performances regarding porosity and sorptivity. Such AAM mortar can considerably increase the lifetime and reduce the maintenance costs of concrete structures.

Disclosure statement

No potential conflict of interest was reported by the authors.

Funding

The authors are grateful to the Investment Program PIA3 of the French State for the grant awarded. We also are grateful the Scientific Program H2020 for Research and Innovation by the European Commission. The authors would also like to acknowledge the Institute of Rennes Chemical Science (ISCR-UMR CNRS 6226) particularly Stephane Freslon from the laboratory Solid Chemistry and Materials of INSA Rennes for provided facilities available.

References

Adam, A. A. (2009). *Strength and durability properties of alkali-activated slag and fly ash-based geopolymer concrete* [Ph.D. thesis]. School of Civil, Environmental and Chemical Engineering, RMIT University.

Albitar, M., Ali, M. M., Visintin, P., & Drechsler, M. (2017). Durability evaluation of geopolymer and conventional concretes. *Construction and Building Materials*, *136*, 374–385. https://doi.org/10.1016/j.conbuildmat.2017.01.056

Aligizaki, K. (2005). *Pore structure of cement-based materials: Testing, interpretation and requirements* (1st ed., p. 432). CRC Press.

Al-Otaib, S. (2008). Durability of concrete incorporating GGBS activated by water-glass. *Construction and Building Materials*, *22*(10), 2059–2067. https://doi.org/10.1016/j.conbuildmat.2007.07.023.

Andrew, R. M. (2018). Global CO_2 emissions from cement production. *Earth System Science Data*, *10*(1), 195–217. https://doi.org/10.5194/essd-10-195-2018

Bildirici, M. E. (2019). Cement production, environmental pollution, and economic growth: Evidence from China and USA. *Clean Technologies and Environmental Policy*, *21*(4), 783–793. https://doi.org/10.1007/ s10098-019-01667-3

Borges, P. H., Banthia, N., Alcamand, H. A., Vasconcelos, W. L., & Nunes, E. H. (2016). Performance of blended metakaolin/blastfurnace slag alkali-activated mortars. *Cement and Concrete Composites*, *71*, 42–52. https://doi.org/10.1016/j.cemconcomp.2016.04.008

Chi, M., & Huang, R. (2013). Binding mechanism and properties of alkali-activated fly ash/slag mortars. *Construction and Building Materials*, *40*(3), 291–298. https://doi.org/10.1016/j.conbuildmat.2012.11.003 Cook, R. A., & Hover, K. C. (1993). Mercury porosimetry of cement-based materials and associated correction factors. *Construction and Building Materials*, *7*(4), 231–240. https://doi.org/10.1016/0950-0618(93)90007-Y

Davidovits, J. (1994). *Properties of geopolymer cements* [Paper presentation]. Proceedings of First International Conference on Alkaline Cements and Concretes, Kiev, Ukraine, p. 131–149 www.geopolymer.org.

Diaz, E. I., Allouche, E. N., & Eklund, S. (2010). Factors affecting the suitability of fly ash as source material for geopolymers. *Fuel*, *89*(5), 992–996. https://doi.org/10.1016/j.fuel.2009.09.012

Duxson, P., Provis, J., Lukey, G., Separovic, F., & van Deventer, J. (2005). 29Si NMR study of structural ordering in aluminosilicate geopolymer gels. *Langmuir 21*(7), 3028–3036. https://doi.org/10.1021/ la047336x

Fernandez, J. A., Torre, A. G., Palomo, A., Olmo, G. L., Alonso, M. M., & Aranda, M. A. G. (2006). Alkali activated materials. *Fuel*, *85*(5–6), 625–634. https://doi.org/10.1016/j.fuel.2005.08.014

Gao, X., Yu, Q. L., & Brouwers, H. J. H. (2015). Properties of alkali activated slag-fly ash blends with lime- stone addition. *Cement and Concrete Composites*, *59*, 119–128. https://doi.org/10.1016/j.cemconcomp.2015.01.007

Granizo, M. L., Alonso, S., Blanco-Varela, M. T., & Palomo, A. (2004). Alkaline activation of metakaolin: effect of calcium hydroxide in the products of reaction. *Journal of the American Ceramic Society*, *85*(1), 225–231. https://doi.org/10.1111/j.1151-2916.2002.tb00070.x

Gu, K., Maierdan, Y., & Chen, B. (2022). Effects of ethylenediamine tetra-acetic acid (EDTA) and its disodium salt derivative (EDTA-Na) on the characteristics of magnesium oxysulfate (MOS) cement. *Composites Part B*, *232*, 109654. https://doi.org/10.1016/j.compositesb.2022.109654

Hagemann, S. E., Gastaldini, A. L. G., Cocco, M., Jahn, S. L., & Terra, L. M. (2019). Synergic effects of the substitution of Portland cement for water treatment plant sludge ash and ground limestone: Technical and economic evaluation. *Journal of Cleaner Production*, *214*, 916–926. https://doi.org/10.1016/j.jclepro.2018.12.324

Hall, C. (1989). Water sorptivity of mortars and concretes: A review. *Magazine of Concrete Research*. *41*(147), 51–61. https://doi.org/10.1680/macr.1989.41.147.51

Hall, C., & Tse, T. K. M. (1986). Water movement in porous building materials-VII, The sorptivity of mortars. *Building and Environment*, *21*(2), 113–118. https://doi.org/10.1016/0360-1323(86)90017-X

Hall, C., & Yau, M. H. R. (1987). Water movement in porous building materials-IX. The water absorption and sorptivity of concretes. *Building and Environment*, *22*(1), 77–82. https://doi.org/10.1016/0360-1323(87)90044-8

Balayssac, J. P. (1993). *Relations entre performances mécaniques, microstructure et durabilité des bétons* [Thèse de doctorat]. INSA Toulouse.

Li, C., Sun, H., & Li, L. (2010). A review: The comparison between alkali-activated slag (Si Ca) and metakaolin (Si Al) cements. *Cement and Concrete Research*, *40*(9), 1341–1349. https://doi.org/10.1016/j.cemconres.2010.03.020

Mackenzie, K. J. D., & Welter, M. (2014). Geopolymer (aluminosilicate) composites: Synthesis, properties and applications. In I. M. Low (Ed.), *Advances in ceramic matrix composites* (pp. 445–470). Elsevier. https://doi.org/10.1533/9780857098825.3.445

Mermerdaş, K., Manguri, S., Nassani, D. E., & Oleiwi, S. M. (2017). Effect of aggregate properties on the mechanical and absorption characteristics of geopolymer mortar. *Engineering Science and Technology, an International Journal*, *20*(6), 1642–1652. https://doi.org/10.1016/j.jestch.2017.11.009

NF EN 13057. (2005). *Test methods – Determination of resistance of capillary absorption*. AFNOR: Association Francaise de Normalisation.

NF EN 196-1. (2005). *Methods of testing cement, Part 1: Determination of strength* (pp. 1–33).

Pacheco-Torgal, F., Abdollahnejad, Z., Camões, A. F., Jamshidi, M., & Ding, Y. (2012). Durability of alkali- activated binders: A clear advantage over Portland cement or an unproven issue. *Construction and Building Materials*, *30*, 400–405. https://doi.org/10.1016/j.conbuildmat.2011.12.017

Provis, J. L., Myers, R. J., White, C. E., Rose, V., & van Deventer, J. S. J. (2012). X-ray microtomography shows pore structure and tortuosity in alkali-activated binders. *Cement and Concrete Research*, *42*(6), 855–864. https://doi.org/10.1016/j.cemconres.2012.03.004

Provis, J., & Van Deventer, J. (2009). *Geopolymers: Structure*, *processing, properties and industrial applica- tions*. Woodhead Publishing Limited.

Provis, J., & van Deventer, J. (2014). *Alkali activated materials, state of the art report*. Springer. https://doi.org/10.1007/978-94-007-7672-2.

Sarathy, R. V., & Dhinakaran, G. (2014). Strength and durability characteristics of GGBFS based HPC. *Asian Journal of Applied Sciences*, *7*(4), 224–231. https://doi.org/10.3923/ajaps.2014.224.231

Shi, C., & Qian, J. (2000). High performance cementing materials from industrial slags – A review. *Resources, Conservation and Recycling*, *29*(3), 195–207. https://doi.org/10.1016/S0921-3449(99)00060-9 Shi, C., Krivenko, P. V., & Roy, D. M. (2006). *Alkali-activated*. Cements and Concrete, Taylor & Francis. https://doi.org/10.1201/9781482266900

Song, J.-K., Yang, K.-H., Kim, G.-W., Lee, C.-T., Kim, B.-J., & Lee, J.-H. (2010). *Properties of sodium alkali-acti- vated ground granulated blast-furnace slag(GGBS) mortar* [Paper presentation]. First International Conference on Sustainability and the Future FISC, Paper's No. BUE-FISC-107. Egypt, elshourouq, Egypt.

Yip, C. K., Lukey, G. C., & van Deventer, J. S. J. (2005). The coexistence of geopolymeric gel and calcium silicate hydrate at the early stage of alkaline activation. *Cement and Concrete Research*, *35*(9), 1688–1697. https://doi.org/10.1016/j.cemconres.2004.10.042

Yip, C. K., Lukey, G. C., Provis, J. L., & van Deventer, J. S. J. (2008). Effect of calcium silicate sources on geopolymerisation. *Cement and Concrete Research*, *38*(4), 554–564. https://doi.org/10.1016/j.cemconres.2007.11.001

Zhang, Z., Provis, J. L., Reid, A., & Wang, H. (2014). Geopolymer foam concrete: An emerging material for sustainable construction. *Construction and Building Materials*. *56*, 113–127. https://doi.org/10.1016/j.conbuildmat.2014.01.081